

Matrix elements for $4d_{5/2}$ photoionization in xenon derived from coincidence electron spectrometry

S J Schaphorst[†], Q Qian[‡], B Krässig[§], P van Kampen^{||}, N Scherer and V Schmidt

Fakultät für Physik, Universität Freiburg, D-79104 Freiburg, Germany

Received 19 June 1997

Abstract. The magnitudes and relative phases of the matrix elements pertaining to $4d_{5/2}$ photoionization in xenon at 132.2 eV photon energy have been derived from observables in an angle-resolved electron spectrometry experiment. The observables in question are the partial cross section, the angular distribution parameter of the photoelectron, the alignment parameter of the photoion, and the angular correlation between the $4d_{5/2}$ photoelectron and the coincident $N_5-O_{2,3}O_{2,3}^1S_0$ Auger electron. Difficulties in extracting the desired matrix elements from these observables are discussed. Despite these difficulties, a set of matrix elements and relative phases could be extracted which is in good agreement with all experimental observables and also fulfils the constraint that spin-orbit effects in the photoelectron's partial waves be negligible. This data set differs significantly from theoretical predictions from relativistic random-phase calculations.

1. Introduction

The extraction of matrix elements (and their relative phases) from a set of independent experimental observables is an interesting problem because it provides, within a certain model, a complete description of the underlying process (Heinzmann 1980, Kessler 1981). In the present case we consider the matrix elements of $4d_{5/2}$ photoionization in xenon in the dipole approximation, which are given by the complex quantities D_+ , D_0 , and D_- associated with the channels $4d^{-1}2D_{5/2}\epsilon f_{7/2}$ $J = 1$, $4d^{-1}2D_{5/2}\epsilon f_{5/2}$ $J = 1$, and $4d^{-1}2D_{5/2}\epsilon p_{3/2}$ $J = 1$, respectively. Alternatively, these matrix elements can be given as three magnitudes, d_+ , d_0 , d_- , and two relative phases Δ_{0+} and Δ_{0-} (the third phase difference is the difference between the two others; an absolute phase is irrelevant for observables). Hence, to extract these five quantities from experimental data, one must have at least five independent observables. One method to achieve this complete description is to determine the cross section σ , the angular distribution parameter β_{phe} of the photoelectrons and the three spin-polarization parameters ξ , η , and ζ of the photoelectrons (for the first such study for $4d_{5/2}$ photoionization in xenon at 94.5 eV photon energy see Müller *et al* (1995)). Another method is based on the cross section σ , the angular distribution parameter β_{phe} , the alignment parameter \mathcal{A}_{20} of the photoion, determined via a measurement of the angular

[†] Present address: Delta Information Systems, 300 Welsh Road, Horsham, PA 19044-2273, USA.

[‡] Permanent address: Centre for Modern Analysis, Shantou University, Shantou, Guangdong 515063, People's Republic of China.

[§] Present address: Physics Division, Argonne National Laboratory, Argonne, IL 60439, USA.

^{||} Permanent address: Physics Department, University College Dublin, Belfield, Dublin 4, Ireland.

distribution parameter β_{Ae} of Auger electrons, and information from the angular correlation pattern of photoelectrons measured in coincidence with the electrons from the subsequent Auger decay (Kämmerling and Schmidt 1991). The establishment of a connection between Auger electron emission and photoionization matrix elements rests on two facts. First, the two-step description for the process of photoionization and Auger decay applies, because the intermediate state is well defined and the energies of the electrons are different. In a two-step process the quantities belonging to photoionization and Auger decay factorize. Second, in this factorization the part of the Auger decay reduces to a known numerical constant, because the Auger electron is described by a single partial wave in the $N_5\text{-O}_{2,3}\text{O}_{2,3}^1\text{S}_0$ transition selected.

When the results of the first experimental study of the matrix elements and their relative phases for $4d_{5/2}$ photoionization in xenon at a photon energy of 94.5 eV were compared with theoretical predictions, the amplitudes were found to be in approximate agreement, but a striking discrepancy did exist for the relative phases (Johnson and Cheng 1992a, Kämmerling and Schmidt 1992). A detailed reanalysis of the experimental data (Kämmerling and Schmidt 1993) then showed that solving the nonlinear equations which connect the observables with the matrix elements and their relative phases was burdened by the presence of circular components in the incident light (the linear polarization expressed in the Stokes parameter S_1 was measured to be $S_1 = 0.957(5)$; leaving for the Stokes parameter S_3 describing circular polarization a range $-0.3 < S_3 < +0.3$). The detailed analysis showed that the uncertainty in S_3 strongly affects the uncertainty in the relative phases. The average fitted values for the phases are in agreement with the theoretical prediction, but the large error bars do not allow a convincing test of the theoretical calculations.

Information on the relative phase Δ_{0+} is of particular interest. It describes spin-orbit effects between the $\epsilon f_{7/2}$ and $\epsilon f_{5/2}$ partial waves of the photoelectron and has been calculated to be zero at nearly all photon energies (Johnson and Cheng 1992a, b). In contrast, a remarkable phase difference between spin-orbit channels of the photoelectron has been found in the related case of $5p_{3/2}$ photoionization in xenon (Heckenkamp *et al* 1986). This result and the failure of our former experiment to get phase information stimulated us to perform a new study on $4d_{5/2}$ photoionization in xenon with improved experimental conditions.

The paper is organized as follows. First we present the experimental details necessary for providing the set of observables. Second, we consider the general parametrization of observables in terms of the matrix elements and their relative phases, concentrating in particular on the parametrization of the angular correlation between the $4d_{5/2}$ photoelectrons and the $N_5\text{-O}_{2,3}\text{O}_{2,3}^1\text{S}_0$ Auger electrons. We then describe the extraction of matrix elements and relative phases from the set of observables. Finally, we discuss the results, comparing them with the theoretical prediction of a relativistic random-phase approximation (RRPA) calculation.

2. Experimental details

The experiment was performed at the electron storage ring BESSY, Berlin, at the TGM5 undulator beam line, using our instrument designed for energy- and angle-resolved electron-electron coincidence spectrometry (Schwarzkopf and Schmidt 1995). To achieve superior experimental data as compared to the previous experiment (Kämmerling and Schmidt 1991), two essential points were considered. First, instead of using the second harmonic of the undulator radiation, the third harmonic was selected. While even harmonics originate from slightly off-axis radiation, odd harmonics are emitted on the undulator axis. Therefore,

insertion of a small pinhole of 0.75 mm diameter exactly at the undulator axis improved considerably the extraction of only linearly polarized light. In the present case the Stokes parameter S_1 has been measured to be $S_1 > 0.993$ (this value refers to the major axis of the polarization ellipse, the tilt angle λ of this axis against the plane of the electron storage ring was determined to be $\lambda = 0(1)^\circ$). This favourable value was obtained in the third harmonic at a photon energy of 132.2 eV, using an undulator gap of 45 mm. Second, the angular correlation pattern between the photoelectrons and their coincident Auger electrons this time was measured by varying the angle for the detected photoelectron (analyser 1) while keeping the direction of the Auger electron fixed (analyser 2). It has been shown (Kämmerling and Schmidt 1993) that because of the higher orbital angular momenta of the photoelectron ($\ell = 3, 1$) as compared with that of the Auger electron ($\ell = 2$), a richer structure in the angular correlation pattern will be observed using this method. The new set-up can thus be expected to provide more sensitive information on the photoprocess. The fixed electron spectrometer for the Auger electrons was mounted in the plane perpendicular to the photon beam at an angle $\phi_2 = 150^\circ$ with respect to the electric-field vector of the incident light. For this angle it was verified that the dynamical information contained in the angular correlation pattern is not restricted by symmetry constraints as is the case for certain geometries (Végh and Becker 1992, Schmidt 1994).

A procedure different from the previous experiment (Kämmerling and Schmidt 1991) was used to obtain the coincident signal. In the previous experiment the photoelectrons were registered in a spectrometer with a detector slit wide enough to accept the photoelectron line in its entirety at a single setting of the pass energy, and the coincident Auger line was sampled at some discrete points by stepping the pass energy of its analyser. In that case, the correct measure of coincident events was the area of the coincident Auger line. In the present case, the coincident signal $I(E_{\text{pass},1}^0, E_{\text{pass},2}^0)$ was counted at the spectrometer pass energies where each non-coincident electron peak had maximum transmission. This simpler procedure can be applied in the present case at a photon energy of 132.2 eV. Here, unlike the situation of the previous experiment at lower photon energy, angle-dependent distortions of the line shapes of the photoelectron and the Auger electron due to post-collision interaction are negligible, because the photoelectron is considerably faster than the Auger electron (see Kämmerling *et al* 1993 and references therein). The coincident intensity $I(E_{\text{pass},1}^0, E_{\text{pass},2}^0)$ is then described by

$$I(E_{\text{pass},1}^0, E_{\text{pass},2}^0) = \frac{d^2\sigma}{d\hat{k}_1 d\hat{k}_2} N_{\text{ph}} n_v \Delta x T_1 \epsilon_1 T_2 \epsilon_2 F_{\text{coi}}. \quad (1)$$

N_{ph} is the photon flux at the sample (in photons/s), n_v the target density, Δx is the length of the source volume seen by the analysers in the coincidence mode, T_i is the transmission in analyser (i) set to pass energy $E_{\text{pass},i}$, ϵ_i the detection efficiency of the respective channeltron detector. F_{coi} is a factor which takes into account the influences of energy distribution functions in the coincidence experiment. The double-differential cross section $d^2\sigma/(d\hat{k}_1 d\hat{k}_2)$ describes the angle-dependent coincident emission of a $4d_{5/2}$ photoelectron and a $N_5\text{-O}_{2,3}\text{O}_{2,3} \text{ } ^1\text{S}_0$ Auger electron. In the following we write the double-differential cross section as the product

$$\frac{d^2\sigma}{d\hat{k}_1 d\hat{k}_2} = \frac{\omega_A \sigma}{16\pi^2} P(\hat{k}_1, \hat{k}_2), \quad (2)$$

where σ signifies the partial cross section of photoionization, ω_A is the partial Auger yield for the selected transition. The function $P(\hat{k}_1, \hat{k}_2)$ is the angular correlation function for electron emission into the directions \hat{k}_1 (photoelectron) and \hat{k}_2 (Auger electron); $P(\hat{k}_1, \hat{k}_2)$

in this construction is normalized to $P(\hat{k}_1, \hat{k}_2) = 1 + \text{angular terms}$ with the angular terms vanishing for integrations over the directions \hat{k}_1, \hat{k}_2 .

The angular correlation pattern $P(\hat{k}_1, \hat{k}_2)$ is the quantity of interest to be obtained in the coincidence experiment. When extracting it from the experimental data following the prescription in equations (1) and (2), one has to bear in mind that $P(\hat{k}_1, \hat{k}_2)$ is only proportional to the measured coincidence rate $I(E_{\text{pass},1}^0, E_{\text{pass},2}^0)$ so long as all other factors are constant and independent of the angle setting of analyser 1. This is not true for the rotatable double-sector cylindrical mirror analyser used in our experiment. It is designed to image not an entrance slit, but the actual source volume into the detector plane (Derenbach et al 1987). This has the advantage that the *area* of the observed peak at different angle settings does not depend on the actual target size, on target inhomogeneities, on small changes of the nominal ground potential, or small misalignments of the analyser. On the other hand, the *width* of the spectrometer transmission function ΔE_1 does depend on these factors. Consequently, the transmission T_1 for a set pass energy depends on these factors as well, because the area of a peak is proportional to the product $T\Delta E$. The effect in the present experiment is demonstrated in figure 1. In the left-hand part the widths ΔE_1 for the two sectors S_1 and S_2 of the rotatable analyser are shown as a function of the respective angle setting; in the right-hand part the corresponding peak areas (the size of the full circles include the error bars) and, for comparison, a circle representing a constant. It can be seen that $T_1\Delta E_1 = \text{constant}$ holds for both sectors of the rotatable analyser; the slight difference in the two sectors can be attributed to different detection efficiencies and is taken into account by mutual normalization. The angle-dependent transmission can be accounted for in the evaluation of the angular correlation pattern by substituting T_1 in equation (1) with constant/ ΔE_1 and using the experimental values ΔE_1 at each angle shown in the left-hand part of figure 1. The transmission T_2 of the fixed analyser is not affected by the rotation of the rotatable analyser. After compensating for the decrease in photon flux by normalization against a suitable photon intensity signal and combining all constant factors to a common proportionality constant, the desired angular correlation pattern then follows from the experimental data as

$$P(\hat{k}_1, \hat{k}_2) = \text{constant} \times I(E_{\text{pass},1}^0, E_{\text{pass},2}^0)\Delta E_1/F_{\text{coi}}. \quad (3)$$

The factor F_{coi} was calculated similarly as described in Schwarzkopf and Schmidt (1995) for the case of direct double photoionization, approximating the energy distributions of monochromatized light and the spectrometer functions of the electron energy analysers by Gaussian functions. In the present case of a two-step process with a discrete photoline and a discrete Auger line with natural width Γ one obtains

$$F_{\text{coi}} = \sqrt{\frac{\Delta E_1^2 \Delta E_2^2}{\Gamma^2 \Delta E_1^2 + \Gamma^2 \Delta E_2^2 + \Delta E_1^2 \Delta E_2^2 + \Delta E_1^2 \Delta E_{\text{bp}}^2 + \Gamma^2 \Delta E_{\text{bp}}^2}}. \quad (4)$$

F_{coi} was evaluated using $\Delta E_{\text{bp}} = 0.32(2)$ eV for the photon bandpass, $\Gamma = 0.12$ eV for the level width of the intermediate state, $\Delta E_2 = 1.06$ eV for the fixed analyser and the angle-dependent values ΔE_1 from figure 1. The resulting experimental angular correlation pattern is shown in figure 3 as a polar plot of the coincident intensities (full circles with error bars; for a detailed discussion of this figure see section 4).

In addition to the angular correlation pattern, the following other observables have been measured at the photon energy of 132.2 eV selected. The angular distribution parameter β_{phe} of the photoelectrons was determined to $\beta_{\text{phe}}(4d_{5/2}) = 1.54(2)$, and the angular distribution parameter β_{Ae} of the Auger electrons to $\beta_{\text{Ae}} = 0.292(20)$. From the latter value the alignment parameter \mathcal{A}_{20} is obtained, $\mathcal{A}_{20}(4d_{5/2}) = -0.274(19)$ (quantization axis along

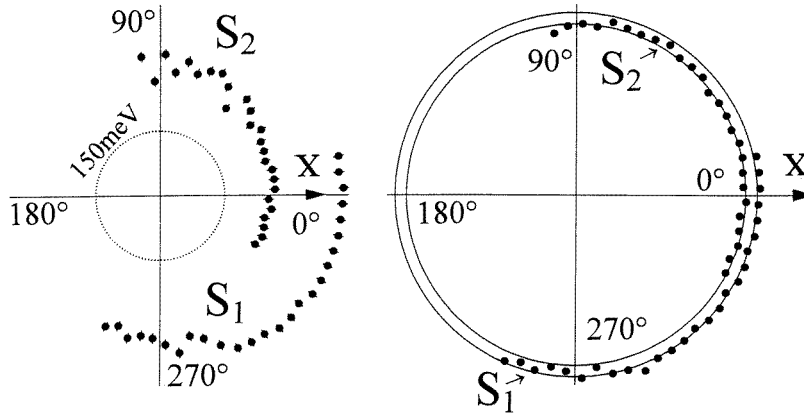


Figure 1. Dependence of characteristic spectrometer parameters on the angle setting of our rotatable analyser. The values displayed have been obtained for $4d_{5/2}$ photoelectrons with 64.7 eV kinetic energy, measured in the two sectors S_1 and S_2 of our photoelectron spectrometer (double-sector cylindrical mirror analyser) which is rotated around the photon-beam direction. Left-hand side: energy resolution ΔE_1 of the electron spectrometer derived from the observed full-width-at-half-maximum value of the $4d_{5/2}$ photoline (after deconvolving the influences of the bandpass of the incident light and the natural level width of the photoionized state); right-hand side: area of the $4d_{5/2}$ photoline, normalized against the angle dependence of these photoelectrons, this value is then proportional to the product of transmission and resolution, $T_1 \Delta E_1$. Experimental data, full circles (error bars on the right-hand side are within the full circles); constant product, circle (full line).

the direction of the electric-field vector of the linearly polarized incident light). The cross section ratios $\sigma(4d_{5/2})/\sigma(4d_{3/2})$ have been measured at 132.2 eV and 94.5 eV photon energy. Together with $\sigma(4d, 94.5 \text{ eV}) = 20.9(10) \text{ Mb}$ (Kammerling *et al* 1989, Becker *et al* 1989) we then get $\sigma(4d_{5/2}, 132.2 \text{ eV}) = 3.0(3) \text{ Mb}$ and $\sigma(4d_{3/2}, 132.2 \text{ eV}) = 2.3(3) \text{ Mb}$.

3. Theoretical parametrizations

The matrix elements (and relative phases) associated with $4d_{5/2}$ photoionization completely describe all observables of present interest, i.e. the partial cross section $\sigma(4d_{5/2})$, the angular distribution parameter $\beta_{\text{phe}}(4d_{5/2})$ of the photoelectron, the alignment parameter $\mathcal{A}_{20}(4d_{5/2})$ of the photoion, and the full angular correlation pattern of $4d_{5/2}$ photoelectrons in coincidence with the $N_5\text{-O}_{2,3}\text{O}_{2,3}^1\text{S}_0$ Auger electrons. The relevant relations will be listed below. They are valid within the dipole approximation; any non-dipole effects, e.g. as observed by Krassig *et al* (1995), are negligible, because all angle-dependent observations in the present case are made in a plane perpendicular to the photon-beam direction. Further, we treat the case of complete linear polarization and select the direction of the electric-field vector of the incident light as the reference axis of a polar coordinate system centred at the sample.

Separating the magnitudes and phases of the matrix elements,

$$\begin{aligned} D_+ &= d_+ e^{i\Delta_+}, & D_0 &= d_0 e^{i\Delta_0}, & D_- &= d_- e^{i\Delta_-}, \\ \Delta_{0-} &= \Delta_0 - \Delta_-, & \Delta_{+-} &= \Delta_+ - \Delta_-, & \Delta_{0+} &= \Delta_{0-} - \Delta_{+-}, \end{aligned} \quad (5)$$

one obtains for the cross section (Huang *et al* 1981; length form of the dipole matrix elements in atomic units; note that the RRPA calculation gives the same results for the

velocity and length form)

$$\sigma(4d_{5/2}) = \frac{4\pi^2\alpha\omega}{3}(d_+^2 + d_0^2 + d_-^2) \quad (6)$$

where ω is the photon energy and α the fine-structure constant. For the angular distribution parameter one finds (Huang *et al* 1981; note several misprints in Kämmerling and Schmidt 1993)

$$\beta(4d_{5/2}) = \left(\frac{1}{5}d_-^2 - \frac{32}{35}d_0^2 + \frac{5}{7}d_+^2 - \frac{6}{5}\sqrt{\frac{2}{7}}d_-d_0 \cos \Delta_{0-} - 12\sqrt{\frac{2}{35}}d_-d_+ \cos \Delta_{+-} + \frac{12}{7}\sqrt{\frac{1}{5}}d_0d_+ \cos \Delta_{0+} \right) / (d_+^2 + d_0^2 + d_-^2), \quad (7)$$

and for the alignment parameter defined in the coordinate system introduced above one gets (Schmidt 1992, p 1502 and equation (A3.4b))

$$A_{20}(4d_{5/2}) = -2(14d_-^2 - 16d_0^2 + 5d_+^2)/(10\sqrt{14}(d_+^2 + d_0^2 + d_-^2)). \quad (8)$$

The observables listed so far are easy to assess. This is not so for the angular correlation pattern. A general expression for the angular correlation has been derived by Kabachnik (1992) using the statistical tensor formalism. In order to facilitate the comparison of the experimental data with this expression, we employ the parametrization for two-electron emission given by Klar and Fehr (1992, equation (19)). For a two-step process the summation indices in the expansion, k_1, k_2 (named ℓ_a, ℓ_b by those authors), are restricted to even values with $k_{1,\max} = 2\ell_1$ and $k_{2,\max} = 2\ell_2$, where ℓ_1 and ℓ_2 are the orbital angular momenta of the photoelectron and the Auger electron, respectively. For linearly polarized incident light the angular correlation between $4d_{5/2}$ photoelectrons and $N_5\text{-O}_{2,3}\text{O}_{2,3}^1\text{S}_0$ Auger electrons in xenon can then be expressed

$$P(\hat{k}_1, \hat{k}_2) = 1 + \alpha_2 P_2(\hat{k}_1 \cdot \hat{k}_2) + \alpha_4 P_4(\hat{k}_1 \cdot \hat{k}_2) + \sum_{k_1, k_2} \beta_{k_1, k_2} B_{20}^{k_1 k_2}(\hat{k}_1, \hat{k}_2). \quad (9)$$

$P_k(\hat{k}_1 \cdot \hat{k}_2)$ are Legendre polynomials, $B_{20}^{k_1 k_2}(\hat{k}_1, \hat{k}_2)$ are bipolar spherical harmonics, and α_k and β_{k_1, k_2} are expansion coefficients. The relation provides a convenient separation between *geometry*, contained in the angle-dependent functions, and *dynamics*, contained in the expansion coefficients. The relation between these expansion coefficients and the matrix elements and phases is established in a lengthy calculation by comparing corresponding angular terms in this parametrization with those in the derivation given by Kabachnik (1992; see also Kämmerling and Schmidt 1993, identifying the reduced matrix elements $\langle j_1 \| E1 \| j_i \rangle$ with the dipole matrix element D_{j_i} of equation (5), with ‘+’, ‘0’ and ‘-’ standing for $j_1 = j_i + 1$, $j_1 = j_i$ and $j_1 = j_i - 1$, respectively). Due to the extent and great complexity of these expressions, we limit the discussion to the special case of electron emission in the plane perpendicular to the photon beam studied in our experiment.

The directions \hat{k}_i in the plane of the experiment are given by single angles ϕ_i , with $0 \leq \phi_i < 2\pi$. The parametrized form of the angular correlation then simplifies to

$$P(\phi_1, \phi_2) = \sum_{k_1, k_2} A_{k_1, k_2} \cos(k_1\phi_1 - k_2\phi_2). \quad (10)$$

The indices k_1 and k_2 are the same as in equation (9), but in this representation they must also fulfil $|k_1 - k_2| \leq 2$. The coefficients A_{k_1, k_2} are combinations of the α_k and β_{k_1, k_2} in equation (9); note that $A_{00} \neq 1$ after equation (9) has been recast in this way. The relation between the coefficients A_{k_1, k_2} and the matrix elements and relative phases is given by

$$A_{k_1, k_2} = M_1 d_+^2 + M_2 d_0^2 + M_3 d_-^2 + M_4 d_0 d_+ \cos \Delta_{0+} + M_5 d_+ d_- \cos \Delta_{+-} + M_6 d_0 d_- \cos \Delta_{0-}, \quad (11)$$

Table 1. Numerical values of the coefficients M_i in equation (11).

k_1	k_2	M_1	M_2	M_3	M_4	M_5	M_6
0	0	1.050 62	0.279 37	0.928 09	0.090 00	-0.435 76	-0.407 50
0	2	0.100 63	-0.208 34	0.397 76	0.063 54	-0.633 90	0.230 32
2	0	0.369 94	-0.208 34	0.066 30	0.545 30	-1.941 22	-0.124 00
2	2	0.651 10	0.359 87	0.397 76	-0.190 56	-0.871 60	-0.566 96
2	4	0.022 20	-0.094 70	0.331 46	-0.013 24	-0.198 10	0.265 76
4	2	0.384 74	-0.094 70	0.0	0.635 30	-0.396 18	-0.088 58
4	4	0.192 37	0.118 39	0.0	-0.238 24	-0.594 26	-0.442 92
6	4	0.258 96	0.0	0.0	0.463 24	0.0	0.0

with the numerical values M_i listed in table 1. Inspection of the table shows that the relative phases Δ_{0+} and Δ_{0-} appear only in cosine functions. Therefore, an ambiguity exists when extracting these phases. For the phase difference Δ_{0-} , for which a finite value has been predicted by theory (Johnson and Cheng 1992b), we adopt the positive sign obtained by these authors.

Application of equation (10) to the present experimental study with fixed direction of the Auger electron, ϕ_2^0 , then leads to the ϕ_1 -dependent angular correlation pattern

$$P(\phi_1, \phi_2^0) = A_0 + A_2 \cos 2\phi_1 + A_4 \cos 4\phi_1 + A_6 \cos 6\phi_1 + B_2 \sin 2\phi_1 + B_4 \sin 4\phi_1 + B_6 \sin 6\phi_1 \tag{12}$$

with the A and B coefficients

$$\begin{aligned} A_0 &= A_{0,0} + A_{0,2} \cos 2\phi_2^0 \\ A_2 &= A_{2,0} + A_{2,2} \cos 2\phi_2^0 + A_{2,4} \cos 4\phi_2^0 \\ B_2 &= A_{2,2} \sin 2\phi_2^0 + A_{2,4} \sin 4\phi_2^0 \\ A_4 &= A_{4,2} \cos 2\phi_2^0 + A_{4,4} \cos 4\phi_2^0 \\ B_4 &= A_{4,2} \sin 2\phi_2^0 + A_{4,4} \sin 4\phi_2^0 \\ A_6 &= A_{6,4} \cos 4\phi_2^0 \\ B_6 &= A_{6,4} \sin 4\phi_2^0. \end{aligned} \tag{13}$$

One can see immediately that the value of coefficient A_6 determines that of B_6 . Furthermore, it can be shown that A_6 itself follows from the other coefficients through the relation

$$A_6 = a_0 A_0 + a_2 A_2 + b_2 B_2 + a_4 A_4 + b_4 B_4 \tag{14}$$

with a_i and b_i depending only on the value of ϕ_2^0 . Hence, our angular correlation pattern is determined by only five independent coefficients, A_0, A_2, B_2, A_4 and B_4 .

4. Extraction of matrix elements

The extraction of the matrix elements d_i and their relative phases $\Delta_{i,j}$ from the experimental data is very much hampered by the strongly correlated way in which these quantities enter into the experimental observables. Because only the partial cross section depends on the *absolute* magnitude of the matrix elements, and because the experimental value of this quantity has the largest error bar, we first use relative values of the matrix elements d_i and normalize these values only in the last step against the experimental partial cross section $\sigma(4d_{5/2})$. The use of relative d_i values does not affect the angular distribution and the

alignment parameter, since these quantities contain d_i in the numerator and denominator, i.e. an overall scaling factor cancels. In contrast, the d_i values play a role for the angular correlation pattern; there the observed pattern, measured on a relative scale, must be multiplied by a constant factor to adapt it to the pattern calculated from a given set d_i and $\Delta_{i,j}$, which is obtained on an absolute scale. This is done by a least-squares fitting procedure.

In the reduction of our data we have followed two strategies. In our first strategy we fit the experimental angular correlation pattern by a least-squares method to the parametrization of equation (12) and extract the five independent parameters A_0 , A_2 , B_2 , A_4 and B_4 . These coefficients are treated as ‘observables’, equivalently to the angular distribution parameter β and the alignment parameter \mathcal{A}_{20} . Hence, we have seven observables O_i and can form seven non-linear equations $F_i = O_{i,\text{calc}} - O_{i,\text{exp}}$ which must be solved for the five unknowns d_+ , d_0 , d_- , Δ_{0+} , and Δ_{0-} . A convenient method is to select initial values for the unknown matrix elements d_i and phases $\Delta_{i,j}$ to get $O_{i,\text{calc}}$ (the method of initial selection is described below), compare these quantities with $O_{i,\text{exp}}$ by calculating the corresponding χ^2 -value, and minimize χ^2 in an iterative procedure by varying the values d_i and $\Delta_{i,j}$. This χ^2 -value then provides a criterion for the quality of agreement that exists between the calculated and the observed quantities O_i and, hence, for the values d_i and $\Delta_{i,j}$ selected (see, e.g., Cumpson and Seah 1992). The application of this strategy was met with serious difficulties which ultimately led us to modify the approach in the way described in the next paragraph. Because the insights gained in the process are of fundamental importance for a successful data treatment, these difficulties will briefly be outlined. It was found that all the angular correlation patterns calculated from initial values d_i and $\Delta_{i,j}$ were less tilted against the polarization axis than the experimental data indicated, independently of the actual d_i and $\Delta_{i,j}$ values used. This discrepancy could be reduced by taking into account two points. First, the tilt of the pattern depends sensitively on the angle ϕ_2^0 ; changing this angle for the calculated pattern by just 1° from $\phi_2^0 = 150^\circ$ to $\phi_2^0 = 149^\circ$, which is within our experimental uncertainty, gives better agreement between the calculated and the observed patterns. Therefore, in our further approaches we take $\phi_2^0 = 149^\circ$. Second, we found that the analyser used at the position ϕ_2^0 , a sector cylindrical mirror analyser with a lens system at its entrance, has a transmission function which depends on the angle under which the electrons actually enter the analyser. This is shown in the left-hand part of figure 2. Hence, for the finite acceptance angles of this analyser a higher transmission exists for electrons with $\phi_2 < \phi_2^0$ than for those with $\phi_2 > \phi_2^0$. In order to correctly take into account this effect, we modified the calculation of the angular correlation pattern by incorporating the finite acceptance angles of both analysers. (The average and opening angles of both analysers, measured in the analyser frame with the z' -axis pointing into the direction of the cylinder axis, are given by $\vartheta_1^0 = 42.8^\circ$, $\varphi_1^0 = 0^\circ$, $\Delta\vartheta_1 = \pm 3^\circ$, $\Delta\varphi_1 = \pm 20^\circ$; $\vartheta_2^0 = 42.3^\circ$, $\varphi_2^0 = 0^\circ$, $\Delta\vartheta_2 = \pm 10^\circ$, $\Delta\varphi_2 = \pm 6^\circ$). This measure improved the agreement between experimental and calculated correlation patterns, concerning their tilt angles, and is applied in all further calculations. At the same time, however, the consideration of finite acceptance angles requires inclusion of the dependences on the out-of-plane angles, which involves the calculation of the angular correlation pattern from more complicated expressions than those given above. Also, it makes the calculation of solid-angle affected A and B coefficients, needed for the comparison with the experimental ones, intractable.

Due to the difficulties arising from the solid-angle effects we developed a second strategy to extract the matrix elements d_i and relative phases $\Delta_{i,j}$. Here we do not seek approximate solutions of the seven nonlinear equations, but concentrate directly on the experimental data of β , \mathcal{A}_{20} together with all experimental points of the angular correlation pattern. Again,

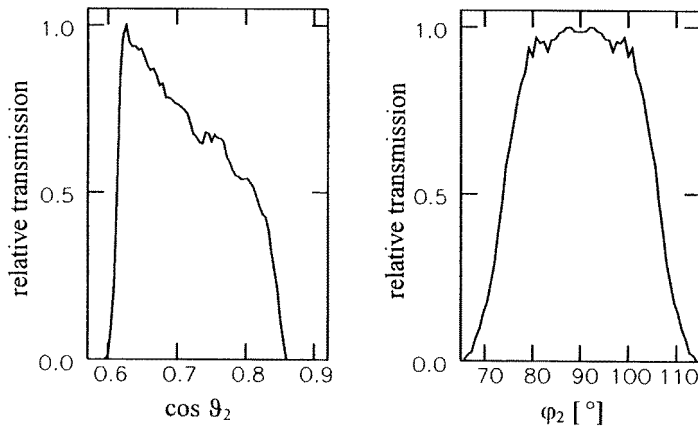


Figure 2. Ray-tracing results for the transmission of our one-sector cylindrical mirror analyser with a lens system at its entrance (Auger electron spectrometer at fixed position). Shown are, for a finite-source volume as seen in the experiment, the dependence of the transmission on the polar and azimuthal angles, ϑ_2 (left-hand side, values are given for $\cos \vartheta_2$) and φ_2 (right-hand side). These angles refer to the reference axis z' which is parallel to the cylinder axis of the analyser. Note that the asymmetry in ϑ_2 results from the acceleration of the electrons in the lens mounted at the spectrometer entrance (no such asymmetry exists in our double-sector cylindrical mirror analyser).

we start with preselected values for d_i and $\Delta_{i,j}$, but then the parameters β and \mathcal{A}_{20} , and the full angular correlation pattern, $\bar{P}(\phi_1, \phi_2^0)$, taking into account in the latter the finite-angle effects (indicated by the bar over the symbol P), are calculated. Because there are two kinds of experimental data, the two parameters β and \mathcal{A}_{20} on the one hand, and the many points of the angular correlation pattern on the other hand, we have tried two slightly different ways to compare the experimental data with the calculated quantities, using the associated χ^2 value as criterion for the quality of the preselected values. In the first one, all data points are treated on an equal footing. In the second one, out of the plethora of preselected d_i and $\Delta_{i,j}$ initial values only those were kept which led to values for β and \mathcal{A}_{20} in agreement with the experimental values (including the error bars). Then we calculated for these combinations of d_i and $\Delta_{i,j}$ the angular correlation patterns $\bar{P}(\phi_1, \phi_2^0)$, taking into account the finite acceptance angles, and compared them with the experimental data, thus obtaining the χ^2 value for the angular correlation pattern only. Both methods yield identical results.

To finish the technical part, our selection of initial values for the matrix elements d_i and relative phases $\Delta_{i,j}$ remains to be explained. First, we consider only a certain range: $-\pi < \Delta_{i,j} < \pi$, and according to equation (6) $d_i^2 < 3\sigma/(4\pi^2\alpha\omega)$ (we allowed twice this value). We then draw five random numbers, one for each of the quantities d_+ , d_0 , d_- , Δ_{0-} and Δ_{+-} to get one set of initial values. With these the observable quantities are calculated and then compared with the corresponding experimental data, thus providing a χ^2 value. We proceed by exploring the neighbourhood of the five-dimensional space of the d_i and $\Delta_{i,j}$ values by allowing gradual changes of the initial values and taking into account all possible combinations between them. For each set of these modified values the calculation of the observables and comparison with the experimental data is repeated until no improvement of the attached χ^2 value can be achieved. The result is a set of matrix elements and relative phases which leads, starting from the initial point, to a local minimum in the χ^2 function.

Table 2. Compilation of parameters needed to describe $4d_{5/2}$ photoionization in xenon at 132.2 eV photon energy. The data of individual lines are described in the main text. Note that for the values obtained from fitting the experimental observables there exists an ambiguity in the sign of the phase differences $\Delta_{i,j}$, i.e. the calculated angular correlation pattern is the same for positive and negative values; guided by theory we present positive values. Note further, that χ^2 is understood to be the reduced value as used in statistical texts which takes into account the number of degrees of freedom (number of measured values minus the number of independently adjustable parameters; in our case there are five adjustable parameters). A good fit typically results in χ^2 being close to unity; the larger values found here are mainly originating from the deviating points at $\phi_1 \approx 38^\circ$ and $\phi_1 = 352^\circ$ which, however, do not affect much the shape of the angular correlation pattern.

Line no	d_+ (au)	d_0 (au)	d_- (au)	Δ_{0-} (rad)	Δ_{+-} (rad)	Δ_{0+} (rad)	σ (Mb)	β	\mathcal{A}_{20}	Constant	χ^2
Experiment											
1							3.0 ± 0.3	1.54 ± 0.02	-0.274 ± 0.019		
Theory											
2	0.654	0.145	0.194	2.27	2.27	0.0	6.35	1.26	-0.256		
3	0.703	0.159	0.205	2.27	2.27	0.0	7.33	1.25	-0.252		
Fit results											
4	0.703	0.081	0.210	3.32	3.06	0.27		1.53	-0.292	80.8	1.42
5	0.703	0.148	0.253	2.76	2.63	0.13		1.54	-0.278	78.4	1.71
6	0.703	0.142	0.253	2.79	2.65	0.14		1.55	-0.282	78.6	1.68
7	0.703	0.160	0.286	2.58	2.51	0.07		1.54	-0.286	76.9	1.72
8	0.703	0.158	0.300	2.68	2.52	0.16		1.56	-0.292	76.5	1.68
9	0.703	0.145	0.258	2.60	2.61	-0.01		1.54	-0.282	78.2	1.71
10	0.703	0.155	0.263	2.80	2.61	0.19		1.55	-0.278	78.1	1.72
11	0.703	0.150	0.271	2.59	2.59	0.00		1.55	-0.284	77.8	1.71
12	0.703	0.145	0.270	2.42	2.58	-0.16		1.54	-0.286	77.8	1.69
13	0.703	0.142	0.250	2.82	2.65	0.17		1.54	-0.280	78.6	1.67
14	0.703	0.153	0.273	2.59	2.57	0.02		1.55	-0.284	77.6	1.71
Change of fit results for $d_0 = 0.159$, $\Delta_{0+} = 0.0$											
15	0.703	0.159	0.301	2.50	2.50	0.0		1.55	-0.292	76.3	1.70
16	0.703	0.159	0.301	2.27	2.27	0.0		1.38	-0.292	74.0	4.52
17	0.703	0.159	0.205	2.50	2.50	0.0		1.37	-0.252	77.7	4.87
Combination occurring most frequently in fit results											
18	0.703	0.15	0.25	2.6	2.6	0.0		1.54	-0.271		
Matrix elements normalized to experimental cross section											
19	0.44	0.10	0.16	2.6	2.6	0.0	3.0	1.54	-0.271		

5. Results and discussion

So far, $4d_{5/2}$ and $4d_{3/2}$ photoionization in xenon is the only example for which theoretical values for the matrix elements and relative phases have been calculated (Johnson and Cheng 1992a, b; for 94.5 eV photon energy see also Liu and Kelly 1992). There are two slightly different data sets, one from a frozen RRP (relativistic random phase approximation) calculation, the other from a relaxed RRP. The relevant data at 132.2 eV photon energy are collected in lines 2 and 3 of table 2, respectively. Also listed are the values for the partial

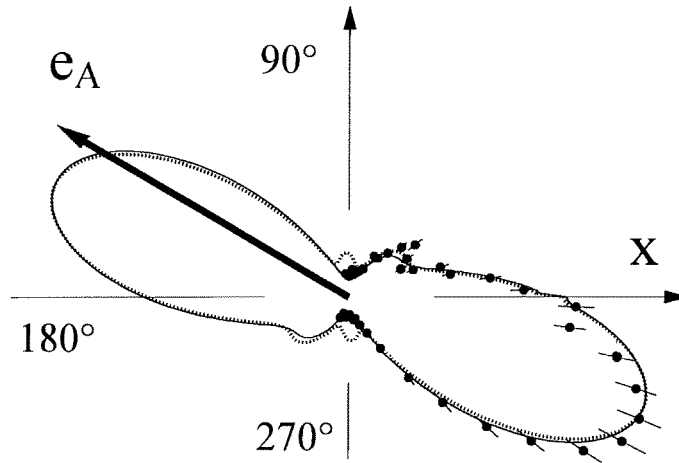


Figure 3. Angular correlation patterns between $4d_{5/2}$ photoelectrons and $N_{5-O_{2,3}}O_{2,3} \ ^1S_0$ Auger electrons in xenon for completely linearly polarized light at 132.2 eV photon energy. Observation is made in a plane perpendicular to the incident photon beam. The direction of the electric field vector is indicated by X , the average direction for the acceptance of Auger electrons at the angle $\phi_2^0 = 149^\circ$ by e_A . The ϕ_1 -dependent intensity of the coincident photoelectron, $P(\phi_1, \phi_2^0)$ of equation (3), is shown as a polar plot. Full circles with error bars, experimental data; dotted and full curves, result from fitting the calculated expression $\bar{P}(\phi_1, \phi_2^0)$ (finite acceptance angles of the electron analysers taken into account) to the experimental values, using the matrix elements and phases of line 3 (relaxed RRPA) and line 4 (best fit to experimental data) in table 2, respectively (for details see text).

cross section, $\sigma(4d_{5/2})$, the angular distribution parameter, $\beta(4d_{5/2})$, and the alignment parameter $\mathcal{A}_{20}(4d_{5/2})$. A comparison of these data with the corresponding experimental values in line 1 leads to the following observations. First, the partial cross section is overestimated by theory by a factor of two. This can be explained by the presence of satellite processes accompanying $4d_{5/2}$ photoionization. They steal intensity from the normal photoprocess, and this effect is not taken into account in the RRPA approach. Second, the theoretical value of the beta parameter is much lower than the experimental value (the theoretical alignment parameter agrees within experimental uncertainties). This indicates a deficiency of the theoretical model concerning the relative magnitudes of the d_i values and/or the relative phases $\Delta_{i,j}$.

Concentrating on the information from the angular correlation pattern, we have to compare in figure 3 the experimental data (points with error bars) with the theoretical calculations (dotted curve which is, within drawing uncertainties, the same for relaxed and unrelaxed RRPA). It can be seen that the theoretical pattern does not describe the experimental data well; the most significant deviation is in the pronounced additional lobes in the theoretical patterns at angles $\phi_1 = 90^\circ$ and $\phi_1 = 270^\circ$.

The aim of the present study is the determination of matrix elements and relative phases from the experimental data. Therefore, we concentrate now on the full curve in figure 3 which represents our best fit to the experimental data using the procedure described in section 4. In the context of comparing the features of a calculated with the experimental angular correlation pattern, one notices a small number of data points, most notably the two points around $\phi_1 \approx 38^\circ$ and the point at $\phi_1 = 352^\circ$ which deviate from the best fit by more than twice their error bars. We have found that in all fits with calculated angular correlation

patterns these points have no significant influence on either the shape of the pattern or the values d_i , $\Delta_{i,j}$, only on the value of χ^2 .

The values for d_i and $\Delta_{i,j}$ which were found in the best fit to the experimental data are collected in line 4 of table 2. The most conspicuous quantity is the relative phase Δ_{0+} with the value 0.27 rad, because, as discussed in the introduction, this phase difference is expected to be zero due to the unimportance of spin-orbit effects between the $\epsilon f_{7/2}$ and $\epsilon f_{5/2}$ partial waves of the photoelectron. Note that the phases Δ_{0-} and Δ_{+-} in this fit settled on opposite sides of π . The fact that the phases enter in the angular correlation only as the arguments of the cosine function renders any determination of the critical relative phase Δ_{0+} the more difficult the closer Δ_{0-} and Δ_{+-} are to π . Because of this particular insensitivity of the fit, the non-zero value found for Δ_{0+} in itself does not yet constitute a strong contradiction to the expectation of negligible spin-orbit effects in the continuum. However, the neglect of such spin-orbit effects has another consequence on the matrix elements. Applying the formulae which transform the matrix elements d_i to radial dipole integrals $R_{\epsilon\ell_j,4d5/2}$ (Schmidt 1992, equation (A.3.23)) and neglecting j -dependences in these radial integrals, one obtains $d_+/d_0 = 2\sqrt{5} = 4.47$. This ratio is in striking contrast to the value of 8.7 found from the above best fit to our data points, which raises the question about the meaningfulness of the values found by indiscriminate minimization of χ^2 .

Because the results obtained from unconstrained minimization of χ^2 are contradictory to the expectation of negligible spin-orbit effects between the $\epsilon f_{7/2}$ and $\epsilon f_{5/2}$ partial waves, we repeated the fitting procedure using constraints more compatible with the expectation of negligible spin-orbit effects in the continuum to further restrict our fitting range to $4 < d_+/d_0 < 5$ and $|\Delta_{0+}| < 0.2$ rad. The 10 data sets with lowest χ^2 values out of 100 randomly selected initial data sets are collected in table 2 (lines 5–14). In comparison to the former result all 100 fits have larger χ^2 values, ranging from $\chi^2 = 1.7$ to $\chi^2 = 2.0$. However, when plotting the corresponding angular correlation patterns one practically cannot, within the accuracy of the drawing, distinguish these patterns from the full curve shown in figure 3. Along with the ratio d_+/d_0 and the phase Δ_{0+} being more compatible with negligible spin-orbit effects in the continuum, also d_- and Δ_{0-} in all 100 data sets are consistently different from the outcome of the unconstrained fit. Clearly, this result indicates that mutual compensation effects exist when the magnitudes and relative phases are changed. The compensation takes place also in the results for the β and \mathcal{A}_{20} parameters.

Notwithstanding fitted data sets for d_i and $\Delta_{i,j}$ being found which are in agreement with the constraints of negligible spin-orbit effects in the continuum, a comparison of these data with the theoretical prediction shows significant discrepancies, also apparent from the differences in the shape of the respective angular correlation patterns. Inspection of table 2 yields that this deviation is greatest for the values d_- and Δ_{0-} . To investigate their influence on the observables we have fixed d_+ , d_0 , Δ_{0+} to the respective RRPA values, $d_+ = 0.703$, $d_0 = 0.159$ and $\Delta_{0+} = 0$, and searched for the remaining values d_- and Δ_{0-} which are in best agreement with the data. The result is shown in line 15 of table 2; in the overall assessment this result has to be given the same weight as each of the 100 fits discussed above. In order to find out which of the values d_- or Δ_{0-} would more improve the agreement between the experimental observables and the theoretical results, we have performed calculations which restrict either Δ_{0-} to the theoretical value (line 16 of table 2) or d_- (line 17). The influence on the angular distribution parameter β and the alignment parameter \mathcal{A}_{20} is listed in table 2 and the influence on the angular correlation parameter is shown in figure 4. Because, within drawing uncertainties, all patterns have the same large lobe, we depict in figure 4 an enlarged view of only the angular range where the RRPA calculation leads to the additional lobe. The figure illustrates that this additional lobe

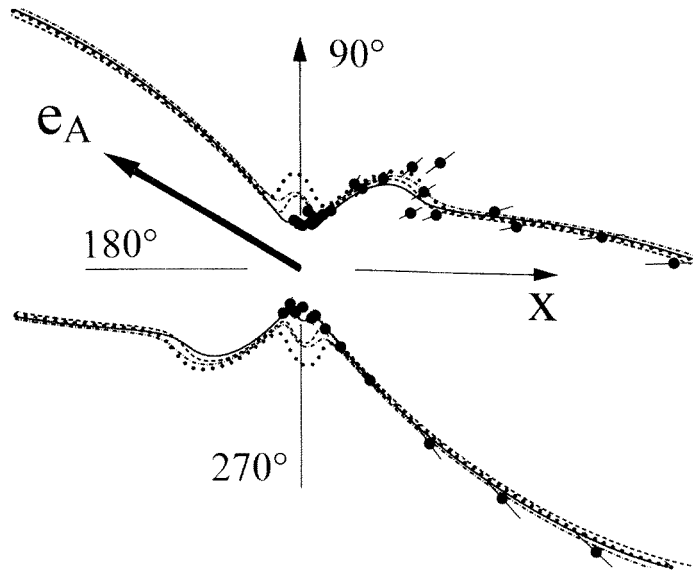


Figure 4. Detail of calculated angular correlation patterns $\bar{P}(\phi_1, \phi_2^0)$ (finite acceptance angles of the electron analysers taken into account) for different values of the photoionization matrix elements and their relative phases. Dotted curve, data from line 3 in table 2 (relaxed RRPA results); chain curve, data from line 16 in table 2 (changed value of d_-); broken curve, data from line 17 in table 2 (changed value of Δ_{0-}); full curve, data from line 15 in table 2 (change of both), this result is within drawing accuracy identical to the full curve shown in figure 3.

disappears gradually when changing d_- from its RRPA value to $d_- = 0.301$ and, similarly, changing Δ_{0-} from its RRPA value to $\Delta_{0-} = 2.50$ rad, but only the combination of both changes leads to the shape consistent with the experimental data.

Taking a closer look at the results from the 100 fit attempts with randomly chosen starting values and upper and lower bounds for d_+/d_0 and Δ_{0+} , one finds that also the fit results for the other quantities spread over certain limited ranges, $0.14 \text{ au} \leq d_0 \leq 0.18 \text{ au}$, $0.20 \text{ au} \leq d_- \leq 0.31 \text{ au}$, $2.4 \text{ rad} \leq |\Delta_{0-}(\Delta_{+-})| \leq \pi$. The distributions of fit outcomes for the individual quantities ranges from being somewhat peaked to being relatively flat, the latter being the case for the critical quantity Δ_{0+} . This may not be taken as a sign that any arbitrary combination of parameters within these ranges reproduces the experimental data points equally well. In contrast, the intercorrelation between any two quantities becomes apparent when plotting the fit results in a two-dimensional histogram. As an example, the correlation between the amplitudes d_- and phases Δ_{+-} , as obtained in the above fits, is reproduced in tabular form in figure 5. Clearly, a smaller value of d_- goes along with a larger value of Δ_{+-} and vice versa. Also, along the ridge one can see an accumulation where the fits with randomized starting values produce certain combinations d_-, Δ_{+-} more frequently than others. For the purpose of obtaining a single result from this investigation, we proceeded with the subset of 37 fits for which the relative phase Δ_{0+} was even more narrowly bounded, $\Delta_{0+} \leq 0.08$ rad, and determined the combinations of the $d_i, \Delta_{i,j}, \beta, \mathcal{A}_{20}$ fit results that occurred most frequently in the two-dimensional histograms for this subset. Analogous to figure 5, the histograms were subdivided into 5–8 bins spanning the above ranges. Within such bin sizes, this procedure produces the unique set of quantities $d_i, \Delta_{i,j}, \beta, \mathcal{A}_{20}$ given in line 18 of table 2. None of these favoured values lies at the edge of the observed ranges, which otherwise would signify a tendency of the fit towards an

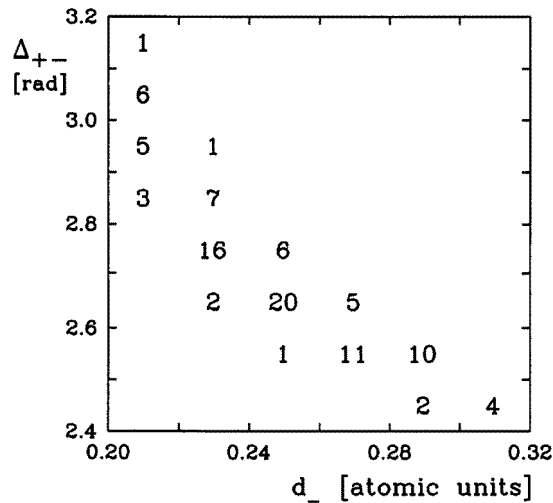


Figure 5. Two-dimensional histogram Δ_{+-} versus d_- (8 bins at 0.1 rad versus 6 bins at 0.02 au) of the results obtained in 100 fit attempts with randomly chosen starting values. The ratio d_+/d_0 and the phase Δ_{0+} in these fits were restricted to the ranges $4.0 \leq d_+/d_0 \leq 5.0$ and $|\Delta_{0+}| \leq 0.2$ rad, respectively.

out-of-bounds result. It is an interesting observation that the ratio d_+/d_0 , being relatively coarsely bounded, comes out close to the value 4.47 quoted above for vanishing spin-orbit effects in the continuum.

As our final result we present in line 19 of table 2 the data from line 18 after normalizing the d_i values to the experimental cross section. This data set is in good agreement with all experimental observables, and it fulfils the requirements imposed by the condition of negligible spin-orbit effects between the $\epsilon f_{7/2}$ and $\epsilon f_{5/2}$ partial waves. While there are ranges for each quantity within which compatibility with the experimental observations is obtained, our analysis yields this particular combination to be favoured by the experimental data. This result can be used as a basis for improved theoretical calculations beyond the present RRPA.

6. Conclusion

Despite their importance as a basic check of theoretical calculations in different approximations, complete experiments in which matrix elements and relative phases are extracted from experimental data are still rather scarce in atomic physics. Related to this scarcity is a limited amount of information on effective and reliable techniques to derive the desired information from complex relations which connect the observables with the matrix elements and phases. For the special case of $4d_{5/2}$ photoionization in xenon with subsequent $N_5-O_{2,3}O_{2,3}^1S_0$ Auger decay we have derived simple expressions for calculating the angular correlation pattern between photoelectrons and Auger electrons: these would also be useful for related studies which may differ in the photon energy and/or electron analyser angle settings. At the photon energy of 132.2 eV we present a detailed analysis of the experimental problems involved with such electron-electron coincidence experiments, and strategies for extracting matrix elements and relative phases from the observables. We have found that the matrix elements and phases obtained from the fit to the angular correlation pattern with

the smallest χ^2 are not compatible with the theoretical assertion that the phase difference Δ_{0+} between the $\epsilon f_{5/2}$ and $\epsilon f_{7/2}$ partial waves be zero. Closer scrutiny of the variation of the fitting parameters revealed that the angular correlation pattern is not uniquely sensitive to this phase difference and that mutual compensation effects between the values of the matrix elements d_i and their relative phases $\Delta_{i,j}$ clearly exist. The experimental data are equally well reproduced with Δ_{0+} fixed to zero, *albeit* leading to a slightly higher χ^2 . The fitted matrix elements which describe all the experimental observables well and which are in agreement with the negligible spin-orbit effects in the photoelectron continuum do, however, differ significantly from the predictions of relaxed and frozen RRPA calculations. These results indicate the need for further refinement of these rather sophisticated calculations.

Acknowledgments

This work was made possible due to important financial support and the collaborative work of several individuals. It is a pleasure to thank the members of BESSY for excellent research facilities, O Schwarzkopf for his help in setting up the experiment, G O'Sullivan for his generosity in supporting the exchange of young researchers (PvK), and H Küst for his advice in fitting procedures. This work has been funded by the Bundesminister für Bildung, Wissenschaft, Forschung und Technologie (BMBF), contract no 055VFAAI, and the Deutsche Forschungsgemeinschaft in the SFB 276, TP B5. SJS thanks the Alexander von Humboldt Stiftung for financial support, QQ the Deutscher Akademischer Austauschdienst for a fellowship, and PvK the European Community for travelling support (Human Capital and Mobility Program, contract no 93-00361).

References

- Becker U, Szostak D, Kerkhoff H G, Kupsch M, Langer B, Wehlitz R, Yagishita A and Hayaishi T 1989 *Phys. Rev. A* **39** 3902
- Cumpton P J and Seah M P 1992 *Surf. Interface Anal.* **18** 345
- Derenbach H, Franke Ch, Malutzki R, Wachter A and Schmidt V 1987 *Z. Phys. A* **260** 258
- Heckenkamp Ch, Schäfers F, Schönhense G and Heinzmann U 1986 *Z. Phys. D* **2** 257
- Heinzmann U 1980 *J. Phys. B: At. Mol. Phys.* **13** 4353
- Huang K N, Johnson W R and Cheng K T 1981 *At. Data Nucl. Data Tables* **26** 33
- Johnson W R and Cheng K T 1992a *Phys. Rev. Lett.* **69** 1144
- 1992b *Phys. Rev. A* **46** 2952
- Kabachnik N M 1992 *J. Phys. B: At. Mol. Opt. Phys.* **25** L389
- Kämmerling B and Schmidt V 1991 *Phys. Rev. Lett.* **67** 1848
- 1992 *Phys. Rev. Lett.* **69** 1145
- 1993 *J. Phys. B: At. Mol. Opt. Phys.* **26** 1141
- Kämmerling B, Kossmann H and Schmidt V 1989 *J. Phys. B: At. Mol. Opt. Phys.* **22** 841
- Kämmerling B, Krässig B and Schmidt V 1993b *J. Phys. B: At. Mol. Opt. Phys.* **26** 261
- Kessler J 1981 *Comment. At. Mol. Phys.* **10** 47
- Klar H and Fehr 1992 *Z. Phys. D* **2** 295
- Krässig B, Jung M, Gemmell D S, Kanter E P, LeBrun T, Southworth S H and Young L 1995 *Phys. Rev. Lett.* **75** 4736
- Liu Z W and Kelly H P 1992 Private communication, cited in Kämmerling and Schmidt (1993)
- Müller N, David R, Snell G, Kuntze R, Drescher M, Böwering N, Stoppmanns P, Yu S-W, Heinzmann U, Viehhaus J, Hergenahn U and Becker U 1995 *J. Electron Spectrosc. Relat. Phenom.* **72** 187
- Schmidt V 1992 *Rep. Prog. Phys.* **55** 1483
- 1994 *Nucl. Instrum. Methods B* **87** 241
- Schwarzkopf O and Schmidt V 1995 *J. Phys. B: At. Mol. Opt. Phys.* **28** 2847
- Végh L and Becker R L 1992 *Phys. Rev. A* **46** 2445